

Accepted Manuscript

Title: Development of a multi-jet polishing process for inner surface finishing

Authors: C.F. Cheung, C.J. Wang, Z.C. Cao, L.T. Ho, M.Y. Liu

PII: S0141-6359(17)30263-5

DOI: <https://doi.org/10.1016/j.precisioneng.2017.11.018>

Reference: PRE 6699

To appear in: *Precision Engineering*

Received date: 5-5-2017

Revised date: 3-9-2017

Accepted date: 22-11-2017



Please cite this article as: Cheung CF, Wang CJ, Cao ZC, Ho LT, Liu M.Y. Development of a multi-jet polishing process for inner surface finishing. *Precision Engineering* <https://doi.org/10.1016/j.precisioneng.2017.11.018>

This is a PDF file of an unedited manuscript that has been accepted for publication. As a service to our customers we are providing this early version of the manuscript. The manuscript will undergo copyediting, typesetting, and review of the resulting proof before it is published in its final form. Please note that during the production process errors may be discovered which could affect the content, and all legal disclaimers that apply to the journal pertain.

Development of a multi-jet polishing process for inner surface finishing

C. F. Cheung *, C.J. Wang, Z.C. Cao, L.T. Ho, M.Y. Liu

Partner State Key Laboratory of Ultra-precision Machining Technology, Department of Industrial and Systems Engineering, The Hong Kong Polytechnic University,
Hung Hom, Kowloon, Hong Kong

*benny.cheung@polyu.edu.hk

Abstract: High-precision inner surfaces are difficult to be machined to a sufficiently high surface quality. This paper presents the development of a novel multi-jet polishing process for precision polishing of inner surfaces through adopting a rod-shaped nozzle designed with a linear array of orifices at its side face. The material removal characteristic on inner cylindrical surface was modelled based on computational fluid dynamic method. Four groups of material removal experiments were conducted to validate the proposed material removal model and investigate its material removal characteristics. Moreover, the surface generation model was also developed and validated based on the material removal model. A series of polishing experiments were conducted on 304 stainless steel cylindrical inner surfaces. The results show that the proposed multi-jet polishing process with the newly designed nozzle is able to achieve high efficiency and precision inner surface finishing on the inner surface.

Keywords: multi-jet tool; inner surface; finishing; fluid jet polishing; abrasive water jet.

1. Introduction

Inner surfaces with a sufficiently high surface quality have been widely used in various industrial fields, such as high-precision optical moulds, aerospace components, automotive systems, and semiconductor plant. The inner surface of X-ray telescopes requires a mirror surface to provide a decent image [1]. The contact surfaces between the inner and outer races of alumina ceramic bearings require a fine surface finish and good form accuracy to reduce the wear rate [2]. Internal passages with poor surface finish can induce undesired boundary layer turbulence in the gas or fluid flowing inside them [3]. Vacuum tubes, wave guides, sanitary tubes [4,5], injectors [6], clean gas bombs and a clean gas piping system [7] are some more examples of components that require a high-precision inner surface finish.

To respond to the needs, some internal surface polishing technologies have been developed. Abrasive flow machining (AFM) was introduced to polish internal channels without detriment to the initial surface profile [8]. However, AFM has limitations in finishing blind holes and achieving uniform finishing of complex internal surfaces. Yamaguchi et al. [9] developed a magnetic abrasive finishing (MAF) which has been successfully adopted to finish inner surfaces of cylindrical components and other complex-shaped samples [10,11]. Despite the promise of producing super mirror finished surfaces, MAF is not suitable for finishing ferromagnetic materials such as nickel and cobalt alloy. Mechanical polishing with a small rod tool was used for inner finishing, but the process is affected by tool wear and tool vibration, especially for machining long tubular surfaces [12].

Although these polishing methods can potentially achieve a good surface quality, they have limitations such as small periodic ripples, surface pollution, significant tool wear, and time-consuming.

There is a need to develop a high-precision inner surface finishing process which can achieve both uniform and good surface finished inner surfaces with high polishing efficiency.

Fluid Jet Polishing (FJP) is one of the promising ultra-precision polishing technologies, which pumps the premixed slurry (abrasive particles and water) through an adjustable nozzle directly towards a target surface at appropriate speeds [13-15]. In recent years, FJP has been widely used in precision polishing of freeform optical glass and moulds, ceramics, etc., depending on its unique advantages, such as high machining accuracy, suitability for polishing of various complex surfaces, undergoes no tool wear and causes no temperature increase of the workpiece during polishing [16-19]. Recently, our group proposed a novel Multi-Jet polishing process and tool to overcome low material removal rate problem of FJP, which can largely enhance the polishing efficiency through integrating a number of orifices in one nozzle [20]. However, the current design of both single jet nozzle and Multi-Jet can hardly be used to polishing the inner surface, especially for the inner surface with high ratio of length to width.

With this in view, a novel design of the Multi-Jet nozzle is developed in this paper to solve this problem. A linearly distributed array of orifices were designed at the side face of a rod-shaped nozzle, which can be easily put into the cavity of the inner surface. Hence, the inner surface can be easily polished through controlling the movement of the rod-shaped nozzle along the length direction of the sample. The finite element model was developed to predict and analyse the material removal characteristics of the multi-jet tool. Hence, the material removal performance was evaluated by a series

of spot tests. Finally, multi-jet polishing process was used for finishing inner cylindrical surfaces. The results show that the MJP process is an effective way for precision polishing of inner surfaces.

2. Multi-jet polishing process and tool for inner surface finishing

Figure 1 shows the schematic diagram of the multi-jet polishing (MJP) process for inner surface finishing by a purposely designed multi-jet (MJ) tool. In the MJP process (see Fig. 1(a)), the workpiece is rotated at a designated rotational speed, while the MJ tool is controlled to move along the generatrix of the inner surface. Different with the MJP tool we recently proposed for high efficiency polishing [20], the MJ tool in this study is designed to be a rod-shaped nozzle with a linear array of orifices at the side face as shown in Fig. 1(b). Hence, it can be put into the chamber of the workpiece to precision polish the inner surface. The pressurized premixed slurry is pumped out from the slurry tank through the nozzle to the inner surface of the workpiece. With the design of an array of orifices on the nozzle, an array of slurry jets are ejected out of the nozzle, and impinge multiple regions on the inner surface simultaneously. Its polishing efficiency is enhanced as compared with the single jet polishing process, and the increase of efficiency is determined by the number of orifices incorporated.

The number and the diameter of the orifices are purposely designed for fitting the need of precision polishing of different types of inner surfaces. Figure 1(b) shows the design of a multi-jet tool with four orifices with a diameter of 0.5 mm which was used for conducting the experiments in this study. The spacing between orifices was 1 mm while the fluid pressure for each orifice was controlled to be up to 10 bars

3. Modelling of material removal characteristics of the multi-jet tool

3.1. Computational fluid dynamic modelling

To predict the material removal of the MJ tool and gain a better understanding of the material removal characteristics, computational fluid dynamic (CFD) modelling was undertaken by using the ANSYS FLUENT software package integrated with the computational fluid dynamic method. Figure 2 shows a schematic diagram of the computational geometrical model of the MJ tool. Figure 2(a) shows the simplified modeling method and boundary conditions. The mixing slurry is pumped into the computational domain through the pressure inlet as shown in right side of Fig. 2(a). Hence, the slurry flows along the cavity inside the MJ tool and the pumped out fluid flow from the orifice array gets through the air environment with a distance defined by the tool offset and finally impinges the target surface. A static pressure of 101325 Pascal was used to set the pressure outlet boundary to signify the environment [21]. Except for the pressure inlet and the pressure outlet defined by the four side surfaces below the orifice array as shown in the right part of Fig. 2(a), other surfaces in the model were defined as no slip wall. ICEM CFD software package was employed as the mesh generation tool. Hexahedral mesh was used to mesh the model, which helped to improve the computational accuracy. To reduce the computing time for the solution, fine grid was specified to some key regions such as the region where fluid jets impinging the target surface as shown in Fig. 2(b). The total number of elements in this mesh model is 918506. The detail geometrical dimensions of this model have also been presented in Fig. 2(b).

The Eulerian-Lagrangian approaches were used to simulate the multiphase flow that involves liquid water, air, and abrasive particles. In the simulation, water and air were treated as Eulerian phases, while the abrasive particle was treated as Lagrangian phase. For turbulence modeling, the Shear-Stress Transport (SST) based on a blending of the $k-\omega$ and $k-\varepsilon$ turbulence models is used to express the turbulent fluid flow in the inner region of the boundary layer as well as in the outer part of the boundary layer for a wide range of the Reynolds number. After the solution of the continuous phase, the influence of the discrete phase was computed by using the discrete phase model (DPM) [22]. One-way coupling was used between fluid and particle motion solution which neglects the particle-particle interaction. Moreover, uniform particle size distribution was assumed to simplify the solution model [19,21]

Oka's erosion model [23] was employed to describe the erosion of the target surface after the impingement of the abrasive particles. The erosion rate $E(\alpha)$ is expressed as:

$$E(\alpha) = g(\alpha)E_{90} \quad (1)$$

$$g(\alpha) = (\sin \alpha)^{n_1} (1 + Hv(1 - \sin \alpha))^{n_2} \quad (2)$$

$$n_1 = s_1(Hv)^{q_1}, n_2 = s_2(Hv)^{q_2} \quad (3)$$

$$E_{90} = K(Hv)^{k_1} (v_p)^{k_2} (d_p)^{k_3} \quad (4)$$

where E_{90} is the erosion rate under normal particle impact, and $g(\alpha)$ denotes the dependence of the impact angle of the normalized erosion. n_1 and n_2 are exponents determined by the material hardness and other impact conditions, Hv is an initial hardness value in GPa units of the target surface. s_1 , s_2 , q_1 , and q_2 are fitting constants for the particle material. K denotes a particle property factor such as

particle shape (angularity) and particle hardness, which has no correlation among different types of particles and other factors; k_1 , k_2 and k_3 are exponent factors, which are affected by other parameters, respectively. Table 1 summarizes the coefficients used in the simulation process and Table 2 shows the material properties of the 304 stainless steel and silicon carbide.

3.2. Simulation results of the computational fluid dynamic model

A simulation experiment was conducted based on the CFD model. The polishing slurry was 4000# SiC with an average size of 3.2 μm and about 6 wt.%. Figure 3 shows the CFD results when the tool offset was 5 mm and the slurry pressure was 6 bars. The velocity of each jet was almost the same before they impinged the target surface. Moreover, their velocity changed due to the interference with the adjacent jet flow as shown in Fig. 3(a), which is attributed to the variation of the polishing spot. Figure 3(b) shows the predicted material erosion depth when the dwell time was 3 minutes. It is observed that the simulated TIF shape is not symmetric even though the distribution of the orifice array is symmetric. This is induced by that the fluid flow pumped into the MJ tool comes from the right side of the nozzle, which is the pressure inlet as shown in Fig. 2(a). It is not symmetric to the orifice distribution.

4. Evaluation of the material removal performance of the multi-jet tool

4.1. Experimental setup

As shown in Fig. 4(a), the experiments were conducted on an IRP200 7-axis ultra-precision polishing machine from ZEEKO Ltd. in the UK. The MJ tool was mounted at the tool spindle through a connection component. Hence, the workpiece was mounted on the chuck of the work spindle which was controlled to move in X/Y/Z directions relative to the MJ tool. The workpiece was rotated through control of the C axis. The cylindrical inner surface (see Fig. 4(b)) was used as the workpiece surface in this study. The material of the workpiece was 304 stainless steel, and its inner surface with a diameter of 40 mm was ground by a Nanoform 450 ultra-precision grinding machine from Moore Nanotechnology System in the USA before the polishing experiments to minimize or even eliminate the effect due to the initial form error.

4.2. Material removal performance

To evaluate the performance of the MJ tool for precision polishing of inner surfaces, four groups of experiments were designed to generate the tool influence function (TIF) under various polishing conditions (see Table 3). They included Group 1: TIF repeatability test, Group 2: TIF test under different tool offsets, Group 3: TIF test under different fluid pressure, and Group 4: TIF test under different dwell times, respectively. For Group 1, eight TIFs were generated. Four of them were generated with a time interval of 10 minutes while the other four were generated with a time interval of 30 minutes. The polishing slurry was 4000# silicon carbide (SiC) abrasive mixed with pure water.

After the generation experiments of TIF, the workpieces were cut into several pieces and they were measured by a Zygo NexView 3D optical surface profiler. Figure 5(a) shows one piece of the cut sample with the polished TIFs on it. Figure 5(b) to Fig. 5(d) show the shape of one of the TIFs generated under the conditions of Group 1 as shown in Table 1 including the raw TIF shape, TIF shape with the removed cylindrical form and the sectional profile, respectively. Induced by the flow jet interference [16], the generated spot shape of each jet is not a symmetrical circular shape as compared to traditional fluid jet polishing, while their material removal depth was close to each other. Figure 5(e) shows the results of the repeatability test. The average material removal depth was used to describe its material removal rate (MRR). It was found that the TIF of MJP had very good repeatability during the test time of 150 minutes, since the variation of the average removal depth was within $\pm 10\%$.

According to the conditions for Group 2, Group 3, and Group 4, Fig. 6 shows that the results of the average material removal depth of the TIF varied under different tool offsets, pressure and dwell time, respectively. Moreover, the simulation under these conditions based on the TIF model in section 3 were also conducted and compared to the experimental results as shown in Fig. 6. It is interesting to note that the variation of the removal depth of the simulated results has good agreement with the experimental results. The effect of the tool offset on the MRR was much smaller than the effect of the slurry pressure according to a comparison of the results in Fig. 6(a) and Fig. 6(b). As shown in Fig. 6(b), the MRR was higher with increasing slurry pressure. The average removal depth exhibited a linear relationship to the dwell time as shown in Fig. 6(c). This implies that the material removal of

the MJ tool was accurately controlled through controlling the dwell time, which is crucial for uniform and deterministic polishing.

Except for the average material removal depth, the shapes of the section profiles of the simulated and experimental TIFs were compared in Fig. 7. The result indicates that the profile of the simulated TIF agrees well with the experimental results, which further verifies the effectiveness of the proposed TIF model. Besides, it is interesting to note that there exist linear grooves between the oval shaped ones in the experimental results as shown in Fig. 5, which was not predicted in the simulation result. The generation reason of this kind of groove may be caused by the particle movement direction changed to along the central line of the adjacent fluid jet after collision. Moreover, their energy can still realize material removal, which leads to this kind of groove. Since the particle-particle interaction was neglected in this model, it cannot predict this kind of groove.

5. Surface generation method of multi-jet polishing of inner cylindrical surface

5.1 Surface generation method

Multi-jet polishing process can also be considered as one of the deterministic polishing process, just like classical fluid jet polishing. In deterministic polishing, the surface generation process is usually considered as the convolution between the dwell time along the tool path and the tool influence function [26,27]. Figure 8 shows the schematic diagram of the surface generation process in multi-jet polishing. Firstly, the simulated three dimensional TIF on cylinder surface was projected to the flat

surface, while practical polishing path for cylinder surface was also projected to the flat surface. Hence, the surface generation model based on the surface generation mechanism of the relative and cumulative removal process [19] was used together with the predicted tool influence function to simulate the surface generation in multi-jet polishing.

5.2 Validation of the surface generation model

In order to validate the effectiveness of the surface generation model, a comparison between the simulated polished surface profile and the measured polished surface profile was also conducted. Table 4 summarizes the polishing conditions and the polishing slurry is 10 wt.% 1000# SiC abrasive. The theoretical material removal distribution was shown in Fig. 9(a) and Fig. 9(b). Combining the theoretical material removal distribution and the initial measured surface profile, the surface profile after polishing can be predicted as shown in Fig. 9(c). The measured surface profile after polishing was also presented in Fig. 9(c). It turns out that the simulated surface profile agrees well with the measured surface profile, which validates the effectiveness of the surface generation model. It is also interesting to note that the surface roughness in the simulated surface form is almost the same with the initial surface form, which is much larger than the practical measured polished surface form. It indicates that this surface generation model cannot be used to predict the surface roughness. It can only be used to predict the surface form.

6. Experimental evaluation of the performance of multi-jet polishing of inner cylindrical surfaces

To evaluate the performance and technological merits of the multi-jet polishing tool and process, a series of polishing experiments was conducted on the inner surfaces of five samples. The experiments were conducted to test the feasibility of multi-jet polishing of inner cylindrical surfaces. To investigate the repeatability of the improvement of surface integrity in terms of uniformity and surface roughness of the inner cylindrical surfaces, five samples were fine ground under the same grinding conditions on a Nanotech 450UPL ultra-precision machine. Hence, they were polished by the multi-jet tool together with 10 wt.% 1000# SiC abrasive slurry. The inner diameter of the cylindrical surface was 40 mm. Table 5 summarizes the polishing conditions of these experiments.

Figure 10 shows the average surface roughness of six surface roughness profiles measured by TAYLOR HOBSON Form Talysurf PGI1240 on sample 1 before and after polishing. Six sectional surface roughness profiles were extracted from each sample as shown in Fig. 10. It is found that the average arithmetic roughness among the six sectional profiles of sample 1 reduced from 48.0 nm to 24.3 nm after one pass of polishing. The cut-off length adopted in the analysis of the surface roughness is 0.25mm, according to ISO 4288-1996. Figure 11 shows a snapshot of sample 1 after polishing. There were three kinds of surface which were fine ground surface, rough ground surface, and polished surface, respectively. Their corresponding surface roughness was measured on the Zygo NexView optical 3D surface profiler. The improvement of the surface finish is conspicuous.

The results of these five samples are presented in Fig. 12. The surface roughness of each sample was determined by averaging the arithmetic roughness values of 6 sectional surface roughness profiles, and the scatter bar shows the fluctuation of the measured value of surface roughness at different positions. The result further implies that the MJP process has high repeatability for improving surface roughness. To demonstrate the uniformity of the MJP process, one of the surface profiles was measured as shown in Fig. 13. This surface profile includes three kinds of profiles, which are the profile after rough cutting, profile after fine grinding and profile after MJP polishing, respectively. Figure 14 shows two different surface profiles before and after one pass of polishing under the polishing conditions as shown in Table 5. It is interesting to note that the initial surface profiles are almost maintained after MJP. Meanwhile, their surface roughness was largely reduced as shown in Fig. 13 and Fig. 14. It demonstrates that MJP also provides good material removal uniformity.

Conclusions

In this paper, a novel multi-jet tool and process for precision polishing of inner surface is presented. A rod-shaped nozzle is designed with a linear array of orifices at the side face, which can be easily put into the cavity of the sample for the polishing of its inner surface. The material removal characteristic was modelled based on the computational fluid dynamic (CFD) method. Four groups of material removal experiments under different conditions were conducted to investigate its material removal

characteristics and validate the material removal model. The result verifies that the proposed material removal model is effective to predict the material removal of MJP. It also indicates that MJP process owns the same material removal characteristics with the classical single jet polishing, which has high material removal stability and controllability. The surface generation model was also developed to predict the polished surface profile. Uniform polishing experiments on the inner cylinder surface were also conducted, and the surface roughness can be quickly reduced to ~20nm after one pass of polishing on stainless steel surface, which proves that the MJP process is technically feasible for precision inner surface finishing. Moreover, the development of the MJP process for inner surface polishing further broadens the machining field of the fluid jet polishing process.

Acknowledgement

The work described in this paper was mainly supported by the funding support to the Partner State Key Laboratories in Hong Kong from the Innovation and Technology Commission (ITC) of the Government of the Hong Kong Special Administrative Region (HKSAR), China. The authors would also like to express their sincerely thanks to the financial support from the Research Office (Project code: BBX7).

References

- [1] Aschenbach B. X-ray telescopes. *Reports on Progress in Physics*. 1985; 48(5):579.
- [2] Bando S, Tsukada A, Kondo Y. A Study on Precision Internal Finishing for Alumina Ceramics Tube. *Jpn Soc Abras Technol*. 2001; 45(1):46-59.
- [3] Ramachandran N, Pande SS, Ramakrishnan N. The role of deburring in manufacturing: A state-of-the-art survey. *Journal of materials processing technology*. 1994; 44(1-2):1-13.
- [4] Kim JD, Kang YH, Bae YH, Lee SW. Development of a magnetic abrasive jet machining system for precision internal polishing of circular tubes. *Journal of materials processing technology*. 1997; 71(3):384-393.
- [5] Wang Y, Hu D. Study on the inner surface finishing of tubing by magnetic abrasive finishing. *International Journal of Machine Tools and Manufacture*. 2005;45(1):43-49.
- [6] Barletta M, Tagliaferri V. Development of an abrasive jet machining system assisted by two fluidized beds for internal polishing of circular tubes. *International Journal of Machine Tools and Manufacture*. 2006; 46(3): 271-283.
- [7] Shinmura T, Yamaguchi H. Study on a new internal finishing process by the application of magnetic abrasive machining: internal finishing of stainless steel tube and clean gas bomb. *JSME international journal*. Ser. C, Dynamics, control, robotics, design and manufacturing. 1995; 38(4):798-804.

- [8] Rhoades L. Abrasive flow machining: a case study. *Journal of Materials Processing Technology*. 1991; 28(1-2):107-116.
- [9] Yamaguchi H, Shinmura T. Study of an internal magnetic abrasive finishing using a pole rotation system: Discussion of the characteristic abrasive behavior. *Precision Engineering*. 2000; 24(3):237-44.
- [10] Yamaguchi H, Shinmura T. Internal finishing process for alumina ceramic components by a magnetic field assisted finishing process. *Precision Engineering*. 2004; 28(2):135-42.
- [11] Yamaguchi H, Nteziyaremye V, Stein M, Li W. Hybrid tool with both fixed-abrasive and loose-abrasive phases. *CIRP Annals-Manufacturing Technology*. 2015; 64(1):337-340.
- [12] Barletta M, Ceccarelli D, Guarino S, Tagliaferri V. Fluidized bed assisted abrasive jet machining (FB-AJM): precision internal finishing of Inconel 718 components. *Journal of Manufacturing Science and Engineering*. 2007; 129(6):1045-1059.
- [13] Faehnle OW, Brug H, Frankena HJ. Fluid jet polishing of optical surfaces. *Appl Opt* 1998;37:6771-37
- [14] Faehnle OW. *Shaping and Finishing of Aspherical Optical Surfaces [dissertation]*, Delft University; 1998.
- [15] Booij SM. *Fluid Jet Polishing-possibilities and Limitations of a New Fabrication Technique [dissertation]*. Delft University;2003.

- [16] Shiou FJ, Asmare A. Parameters optimization on surface roughness improvement of Zerodur optical glass using an innovative rotary abrasive fluid multi-jet polishing process. *Precision Engineering*. 2015 ;42:93-100.
- [17] Zhu HT, Huang CZ, Wang J, Li QL, Che CL. Experimental study on abrasive waterjet polishing for hard–brittle materials. *International Journal of Machine Tools and Manufacture*. 2009;49(7):569-578.
- [18] Beaucamp A, Namba Y. Super-smooth finishing of diamond turned hard X-ray molding dies by combined fluid jet and bonnet polishing. *CIRP Annals-Manufacturing Technology*. 2013; 62(1):315-318.
- [19] Cao ZC, Cheung CF, Ren M. Modelling and characterization of surface generation in Fluid Jet Polishing. *Precision Engineering*. 2016; 43:406-17.
- [20] Wang CJ, Cheung CF, Ho LT, Liu MY, Lee WB. A novel multi-jet polishing process and tool for high-efficiency polishing. *International Journal of Machine Tools and Manufacture*. 2017; 115: 60-73.
- [21] Qi H, Wen D, Yuan Q, Zhang L, Chen Z. Numerical investigation on particle impact erosion in ultrasonic-assisted abrasive slurry jet micro-machining of glasses. *Powder Technology*. 2017; 314: 627-634.
- [22] Mansouri A, Arabnejad H, Shirazi SA, McLaury BS. A combined CFD/experimental methodology for erosion prediction. *Wear*. 2015; 332:1090-7.

[23] Oka YI, Okamura K, Yoshida T. Practical estimation of erosion damage caused by solid particle

impact: Part 1: Effects of impact parameters on a predictive equation. *Wear*. 2005; 259(1):95-101.

[24] Oka YI, Yoshida T. Practical estimation of erosion damage caused by solid particle impact: Part

2: Mechanical properties of materials directly associated with erosion damage. *Wear*. 2005;

259(1):102-9.

[25] <http://www.matweb.com/>

[26] Wang CJ, Yang W, Wang ZZ, Yang X, Hu CL, Zhong B, Guo YB, and Xu Q. Dwell-time

algorithm for polishing large optics. *Applied Optics* 2014 53(21): 4752-4760.

[27] Wang CJ, Wang ZZ, and Xu Q. Unicursal random maze tool path for computer-controlled optical

surfacing. *Applied Optics* 2015 54(34): 10128-10136.

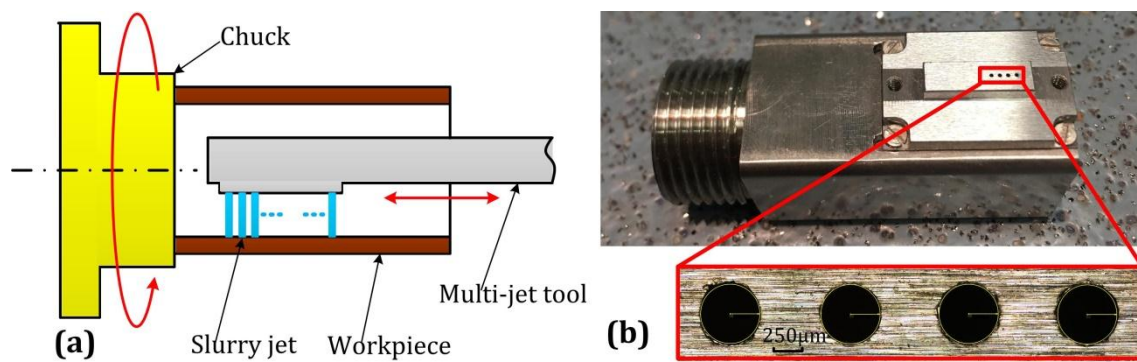


Fig. 1. Schematic diagram of (a) the multi-jet polishing process and (b) multi-jet tool for inner surface finishing.

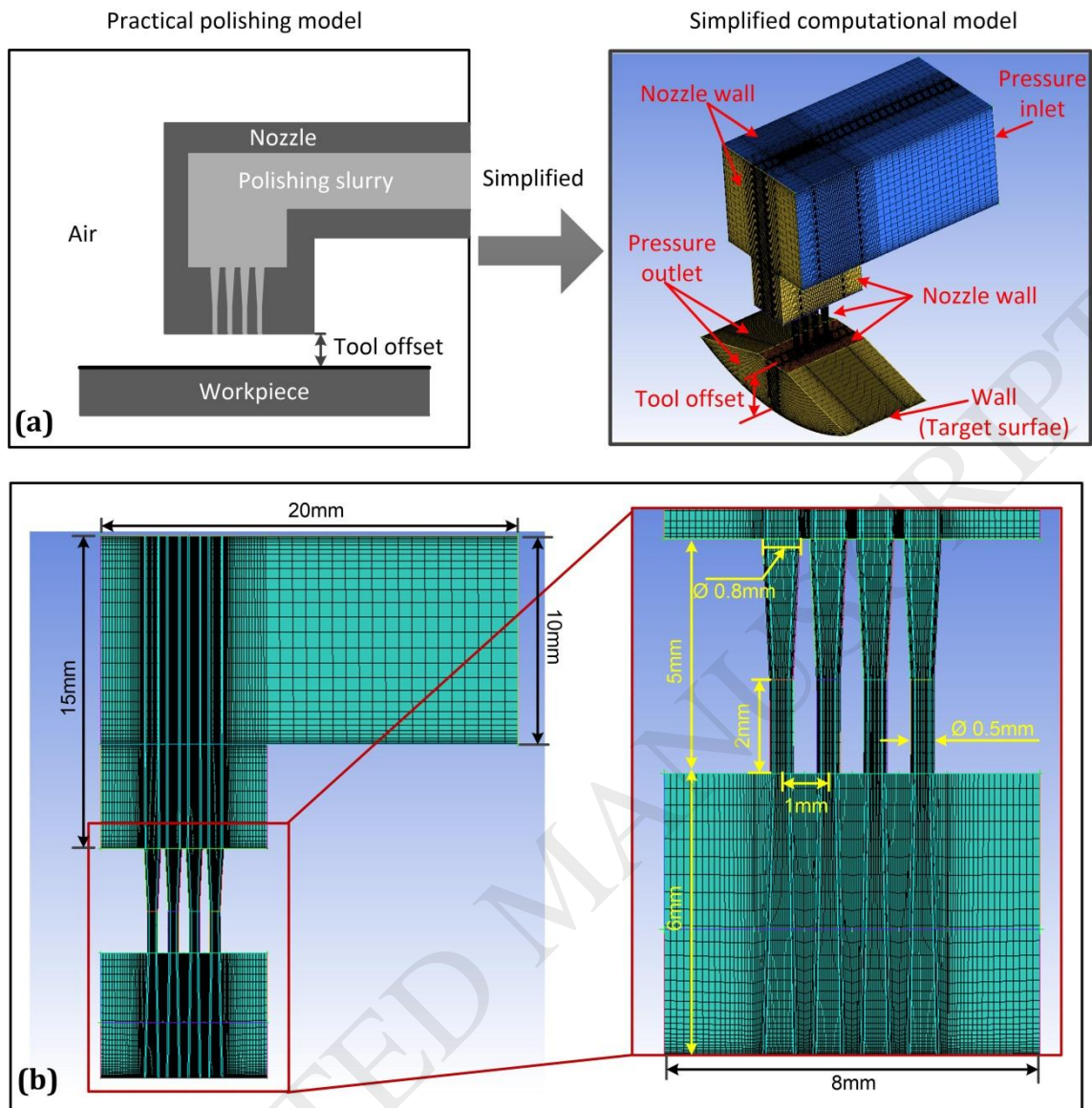


Fig. 2. Schematic diagram of the computational geometrical model: (a) simplified modeling method and boundary

conditions, and (b) sectional view of the model and geometrical dimensions (The tool-offset is 6mm in this case)

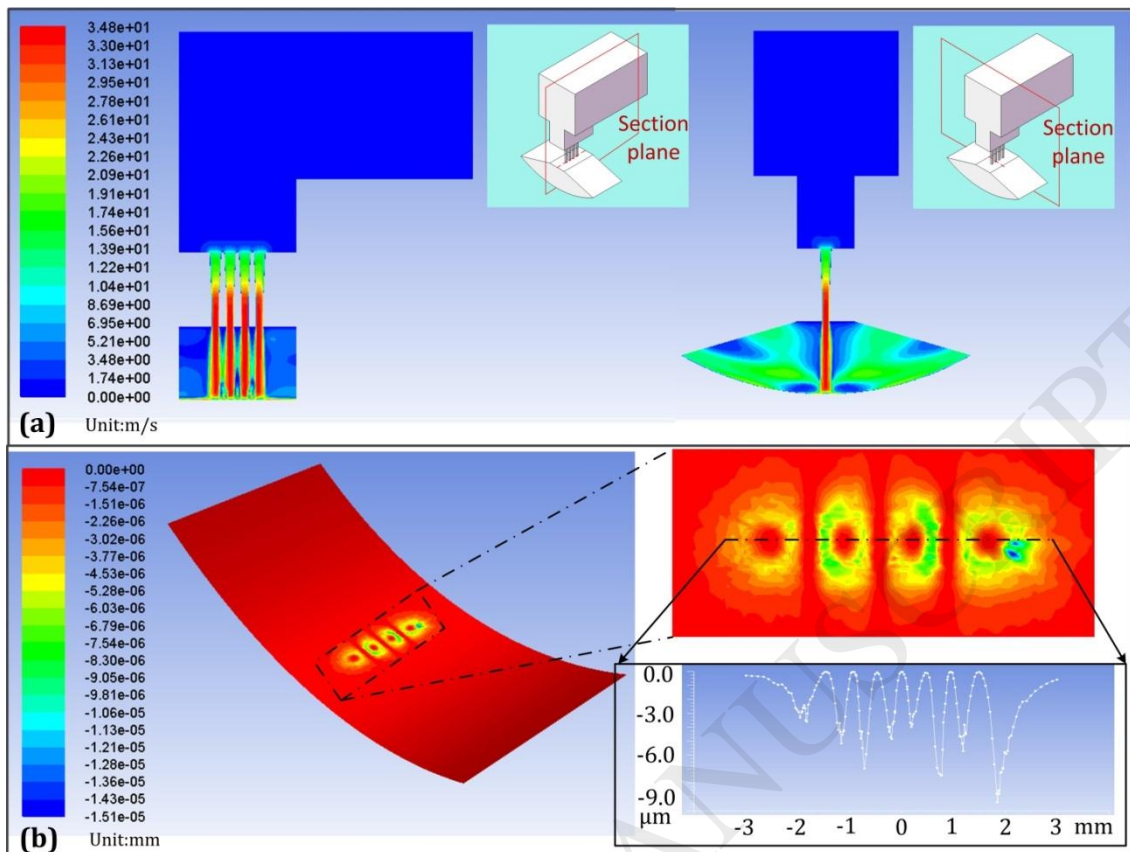


Fig. 3. The CFD results of one of these four cases including the velocity distribution and predicted erosion depth: (a)

two views of the velocity distribution results and (b) predicted erosion depth on the target surface.

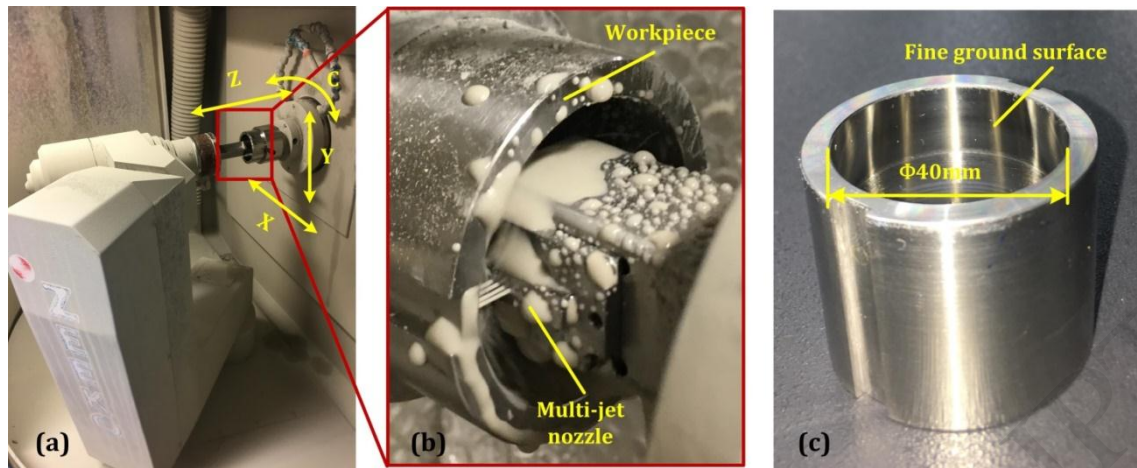


Fig. 4. Snapshots of the experimental setup: (a) experimental device; (b) multi-jet impinging the inner surface and (c) workpiece.

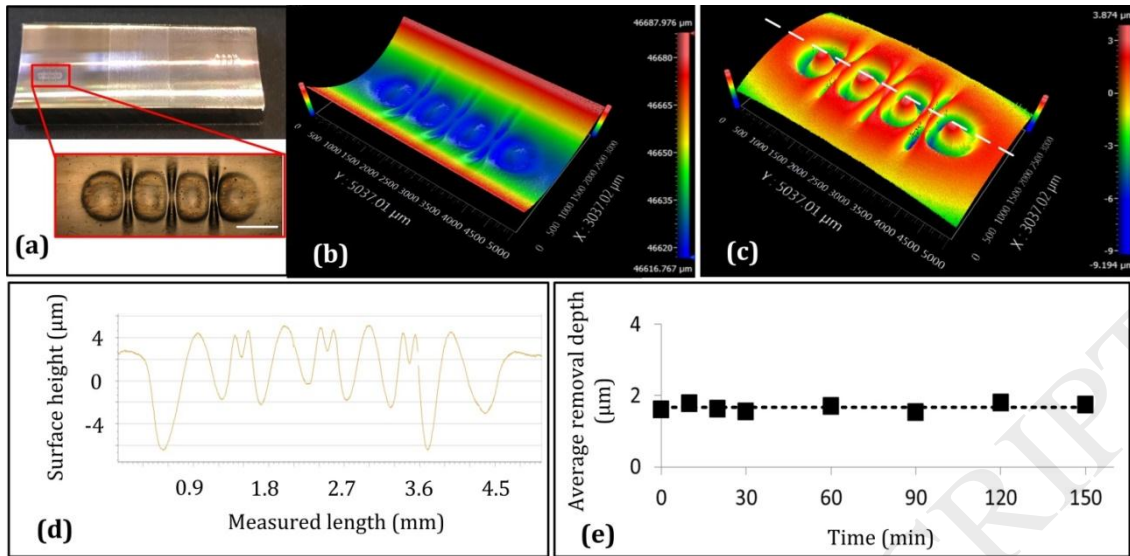


Fig. 5. The generated TIF and its average material removal depth variation with time: (a) snapshot of the TIF (scale bar length: 1 mm); (b) raw contour shape of the generated TIF; (c) contour of the TIF after removing the cylindrical form; (d) the section profile of the TIF along the dotted line as shown in (c) and (e) the average material removal depth of each TIF which varies with time.

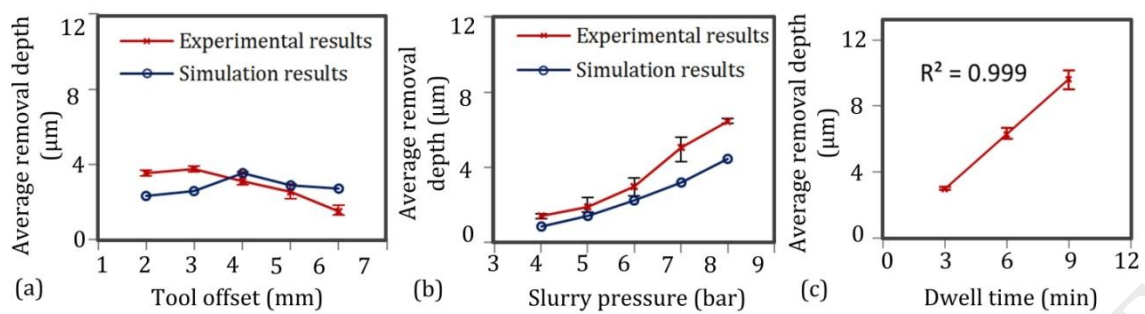


Fig. 6. The relationship between the material removal rate (MRR) of the TIF and the polishing conditions: (a) MRR

varies with tool offset; (b) MRR varies with slurry pressure and (c) MRR varies with the dwell time.

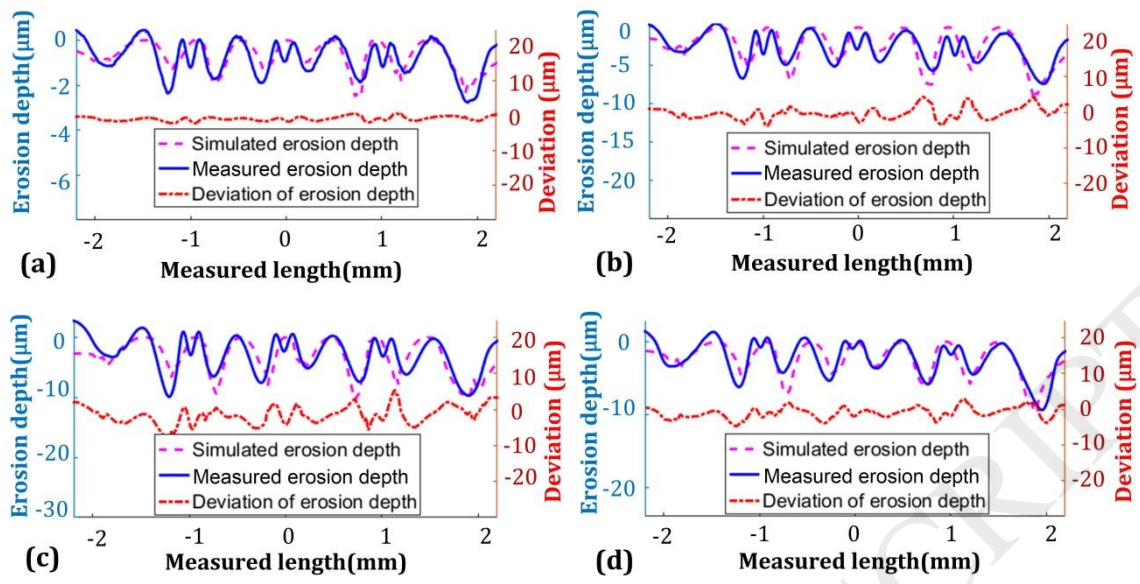


Fig. 7. Simulated and experimental erosion depth of four different cases: (a) slurry pressure=4 bars, tool offset=5 mm;

(b) slurry pressure=6 bars, tool offset=5 mm; (c) slurry pressure=6 bars, tool offset=4 mm and (d) slurry pressure=6

bars, tool offset=6 mm.

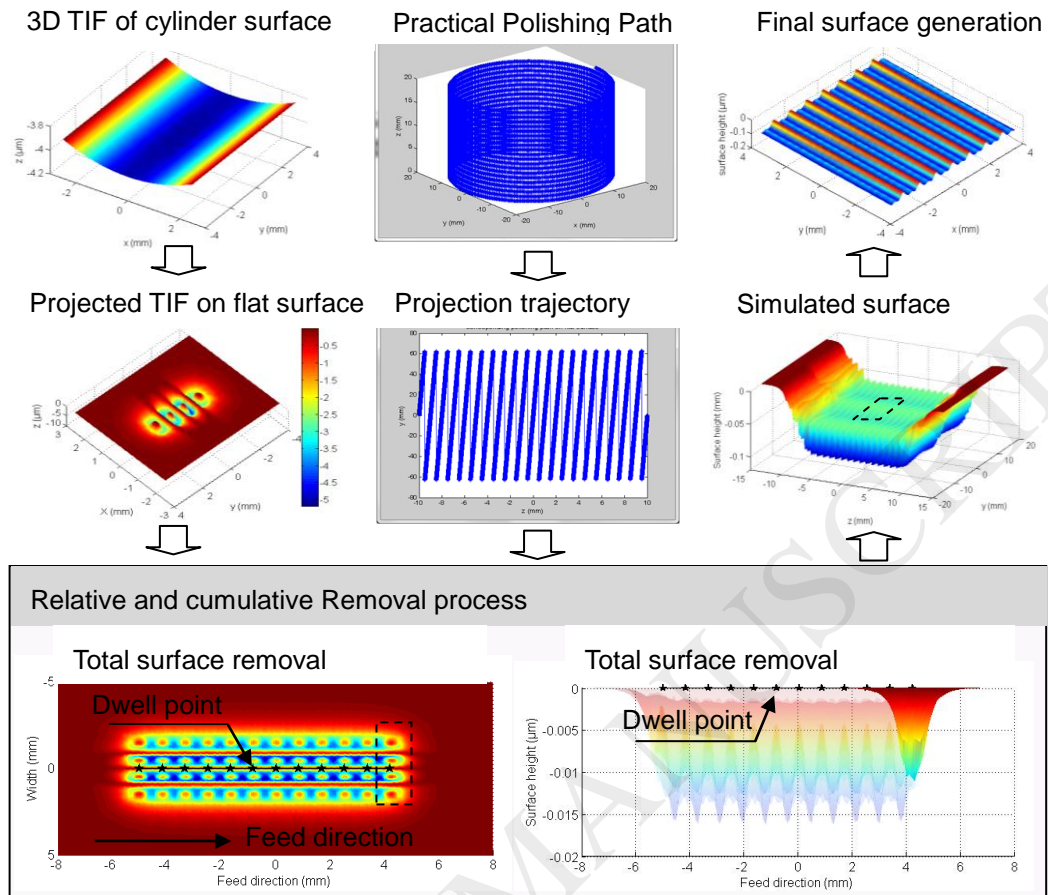


Fig. 8. A schematic diagram of the surface generation process in multi-jet polishing

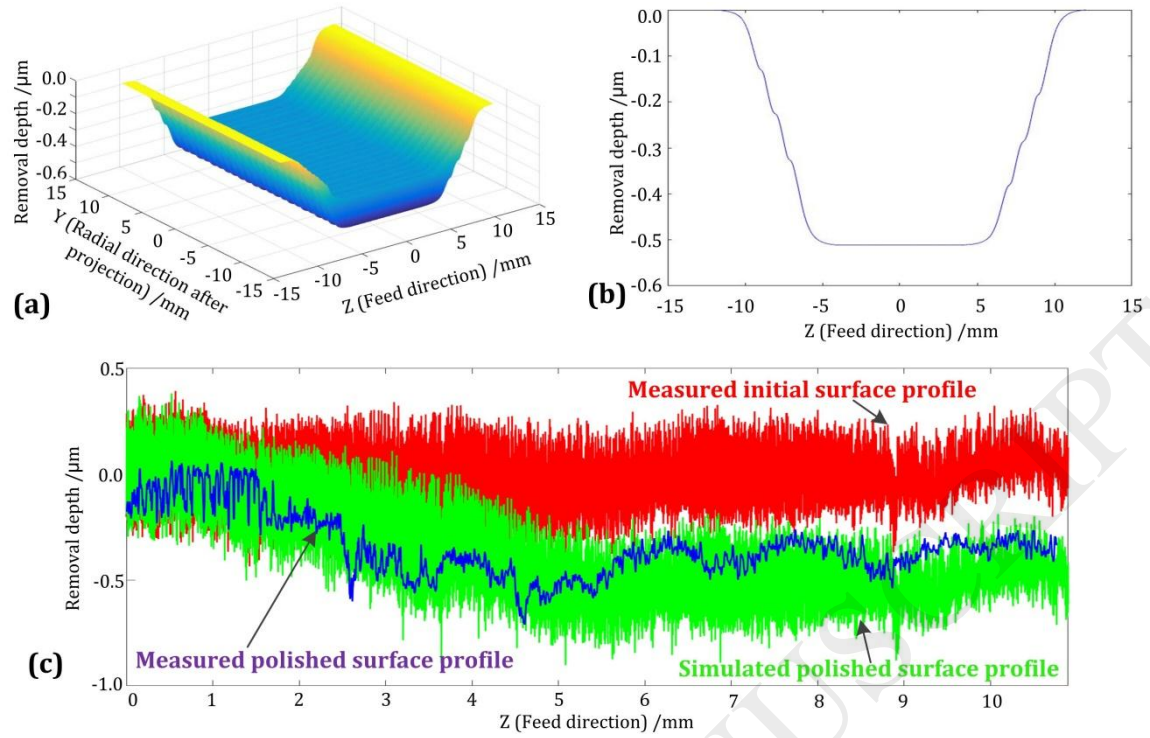


Fig. 9. Comparison of the simulated and measured polished surface profiles: (a) the theoretical material removal distribution of the cylindrical surface after projected to the flat surface; (b) the sectional form profile in (a); (c) sectional profile comparison between the simulated and measured polished surface profiles, and the simulated polished surface profile is based on the measured initial surface profile.

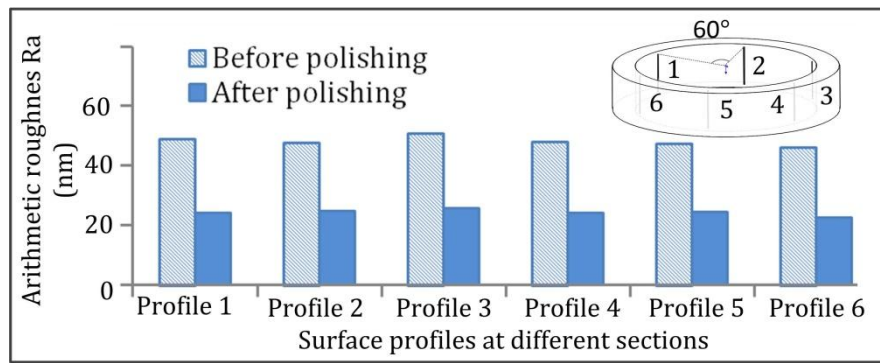


Fig. 10. Surface roughness at the six sectional surface roughness profiles of sample 1 before and after one pass of polishing.

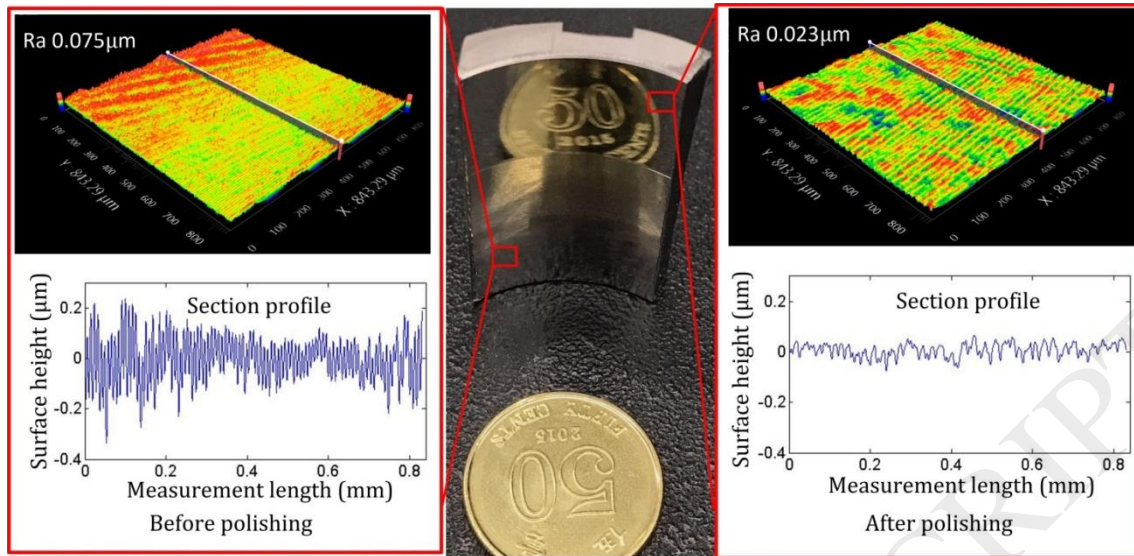


Fig. 11. Snapshot and surface roughness measurement of a segment of sample 1 before and after polishing.

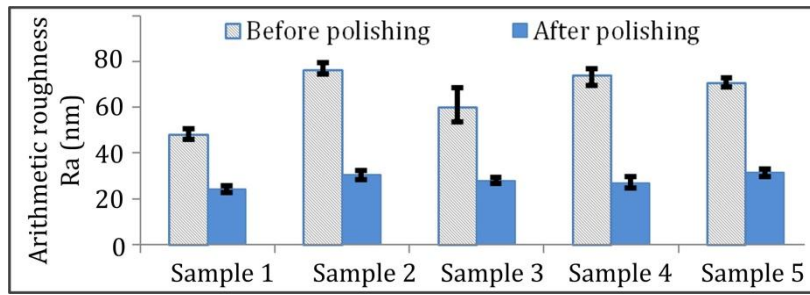


Fig. 12. Surface roughness of 5 different samples before and after one pass of polishing.

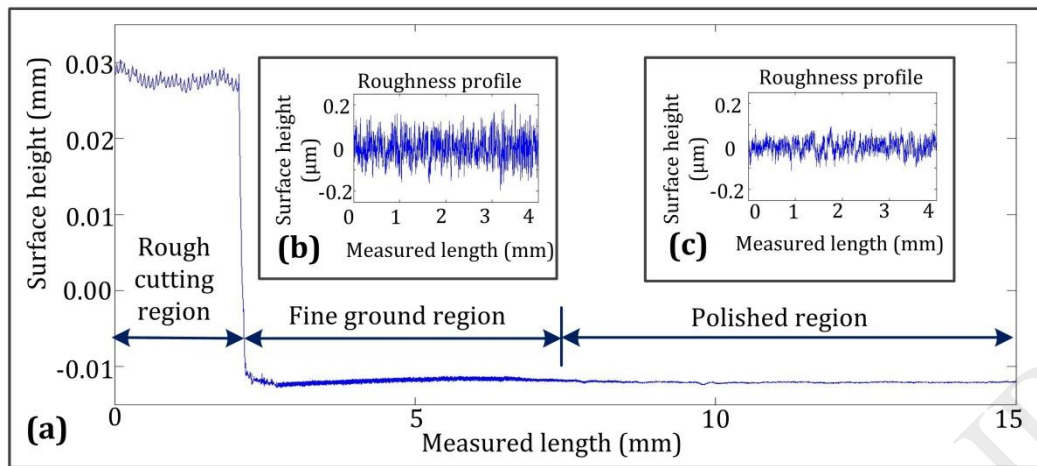


Fig. 13. Comparison of the surface roughness at different stages: (a) surface profile at different stages; (b) after being fine ground and (c) after multi-jet polishing.

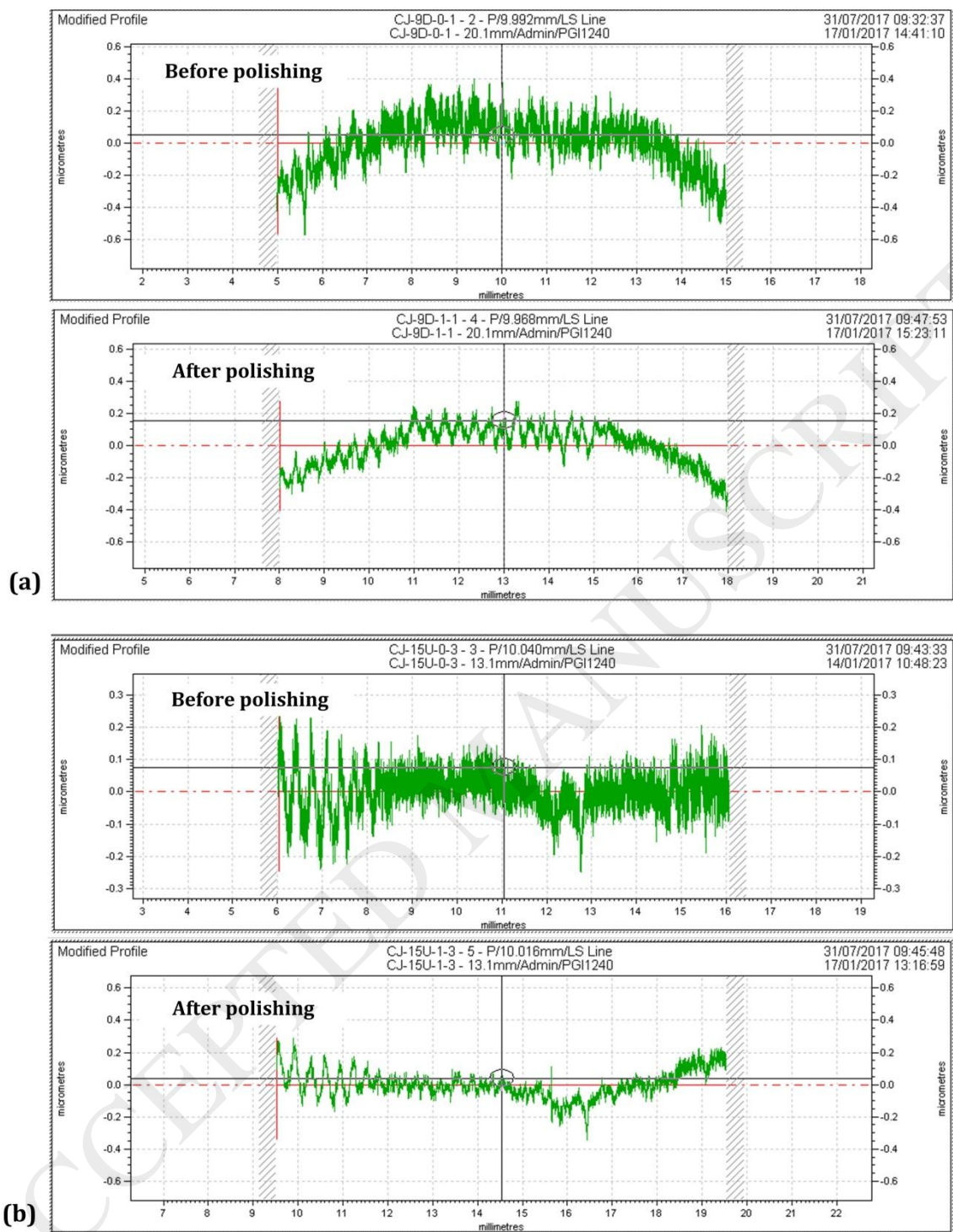


Fig. 14. Two different profiles of the cylindrical surfaces before and after multi-jet polishing: (a) profile 1; (b) profile

Table 1 Coefficients in the erosion model [23,24]

Coefficients	k_1	k_2	k_3	s_1	s_2	q_1	q_2
Value	-0.05	3.31	0.19	0.71	2.80	0.14	-1.00

Table 2 Material properties used in the simulation experiments [25]

Materials	304 stainless steel	Silicon carbide
Density (kg/m ³)	8000	3100
Vicker's hardness (GPa)	3.17	27.45

Table 3 Experimental design for the material removal performance.

Conditions	Group 1	Group 2	Group 3	Group 4
Tool offset (mm)	5	2,3,4,5,6	5	5
Fluid pressure (bar)	6	6	4,5,6,7,8	6
Dwell time (min)	3	3	3	3,6,9
wt.% of the slurry (%)	6	6	6	6

Table 4 Polishing conditions for the validation of surface generation model

Conditions	Values
Tool offset (mm)	5
Fluid pressure (bar)	6
C-axis speed (rpm)	10
Z-axis speed (mm/min)	1
Polishing length along Z direction (mm)	6
Polishing time (min)	6

Table 5 Polishing conditions for the evaluation of the performance of multi-jet polishing of inner cylindrical surfaces.

Conditions	Values
Tool offset (mm)	5
Fluid pressure (bar)	4
C-axis speed (rpm)	10
Z-axis speed (mm/min)	1
Polishing length along Z direction (mm)	15
Polishing time (min)	15